Metallization of self-assembled organic monolayer surfaces by Pd nanocluster deposition

Venäläinen, Annika Elisa

2018-11

Venäläinen , A E , Meinander , N K , Räisänen , M T , Tuboltsev , V & Räisänen , J A 2018 , ' Metallization of self-assembled organic monolayer surfaces by Pd nanocluster deposition ' , Surface Science , vol. 677 , pp. 68-77 . https://doi.org/10.1016/j.susc.2018.06.006

http://hdl.handle.net/10138/238270
https://doi.org/10.1016/j.susc.2018.06.006

Surface Science 677 (2018) 68–77

Contents lists available at ScienceDirect

Surface Science

journal homepage: www.elsevier.com/locate/susc

Metallization of self-assembled organic monolayer surfaces by Pd nanocluster deposition

Annika Venäläinen*,[1,a], Kristoffer Meinander[1,a], Minna Räisänen[b], Vladimir Tuboltsev[a], Jyrki Räisänen[a]

[a] Division of Materials Physics, Department of Physics, University of Helsinki, P.O. Box 43, FI-00014, Finland
[b] Department of Chemistry, University of Helsinki, P.O. Box 55, FI-00014, Finland

ARTICLE INFO

Keywords:
Metallization
Self-assembled monolayer
Pd nanocluster

ABSTRACT

A condensation-cell-type cluster aggregation source was used to deposit Pd clusters on the self-assembled monolayers of four different types of organic molecules. Mica slides covered by Au (111) were coated with self-assembled monolayer films of n-dodecanethiol, 4-mercaptopyridine, dimethyldithiocarbamate, and diethyldithiocarbamate, and the behaviour of Pd clusters on these surfaces, as well as on the bare Au (111) surface, was characterized using scanning tunnelling microscopy and X-ray photoelectron spectroscopy. The aim of this study was to present an alternative means for the metallization of organic layers, through the use of preformed clusters that, unlike single adatoms, are less likely to penetrate the organic layer and cause unwanted interfacial layers or short circuits, and deduce its suitability for the various types of organic self-assembled monolayers. Our experimental results indicate that all of the studied self-assembled monolayers are impenetrable for Pd clusters deposited at thermal energies. Contrary to most methods of metallization, Pd cluster deposition therefore provides an efficient means of growing metal overlayers on organic self-assembled monolayers.

1. Introduction

Self-assembled monolayers (SAMs) of organic molecules on metal surfaces have already diverse applications ranging from molecular sensors [1] to molecular electronics [2–4]. Nanoelectronic devices based on molecular building blocks have also the potential to eventually replace the conventional technologies based on silicon integrated circuits in the future. The crucial point in the electronic applications is the formation of appropriate metallic contacts [5].Therefore metallization of organic surfaces is of great importance in molecular electronics and it has gained much interest in recent years [6–8]. In this respect, the focus has especially been on thiolate SAMs on metals [9].

The metal-molecule interactions are complex and strongly depend on the organic layer and the experimental conditions. Typically, the metal atoms penetrate through the monolayer via structural defects and two-dimensional structures are formed at the SAM-substrate interface thus hindering the preparation of the electrical contacts [10–12]. In most studies reported in the literature, metallization is achieved by electrochemical [13–15], electroless [16–19], or vapour deposition [17,20–22]. The downside with the electrochemical method is that it requires a precise potential control on samples, which also is a challenge for serial production of nanostructured molecular junctions. Electroless deposition on the other hand involves solution electrochemistry as reducing agents are used for metallic adlayer formation. The reducing agents must be carefully chosen to avoid impurities in the final deposit [19]. Vapour deposition techniques found in the literature are based on separate atoms being deposited on the surface and then undergoing possible nucleation. Pulsed laser deposition has been used through nano- and microtencils to deposit patterns of Pt, Pd, Cu and Au on different SAMs [17,20,21], and organometallic chemical vapour deposition has been used to deposit Au on SAMs [22].

In this study, we have chosen to use gas-phase formed clusters for the metallization. This approach of preformed cluster deposition has the advantage of separating the process of cluster nucleation from surface interactions and dynamics on the surface. This allows a greater control over the properties of the final surface-supported clusters [12,17] while at the same time limiting the possibility for single adatoms to penetrate through the organic SAM. All metal atoms are bound to the clusters and single adatoms that more easily diffuse on the surface and penetrate through the SAMs do therefore not appear. The aim of this study was to prepare structures where Pd clusters are immobilized on top of different SAMs to create much sought after metal-

* Corresponding author.
E-mail address: annika.venalainen@helsinki.fi (A. Venäläinen).
[1] These authors contributed equally to this work.

https://doi.org/10.1016/j.susc.2018.06.006
Received 14 December 2017; Received in revised form 6 June 2018; Accepted 13 June 2018

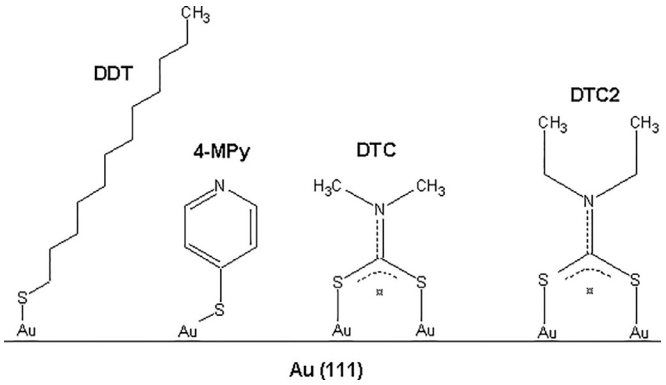

Fig. 1. SAMs of n-dodecanethiol (DDT), 4-mercaptopyridine (4-MPy), dithiocarbamate (DTC) and diethyldithiocarbamate (DTC2) on Au(111).

SAM-metal structures.

In our previous studies we have deposited coinage metal clusters on *n*-dodecanethiolate (DDT) SAMs [12,23]. Now we wanted to extend the cluster deposition studies on different types of SAMs as such systematic studies have so far been lacking in the literature. Pd clusters have diverse applications for example as hydrogen sensors [24] and catalysts [25]. To our knowledge there are no reports on gas-phase Pd cluster deposition on SAMs. Thereby Pd clusters were deposited on DDT, 4-mercaptopyridine (4-MPy), dimethyldithiocarbamate (DTC) and diethyldithiocarbamate (DTC2) SAMs on Au(111) as well as on bare Au itself. The schematic structures of the SAMs are shown in Fig. 1.

DDT SAM was chosen since alkanethiols, which are the most commonly used and studied molecules for SAMs, provide good model systems for both fundamental and applied research [9]. Alkanethiol SAMs are well-packed and ordered as well as stable and robust under various conditions [26]. The surface coverage of dithiocarbamates on Au(111) is comparable to that of alkanethiols (although different in respect of rate and adsorption concentration) [27] and under ambient conditions dithiocarbamate SAMs on Au can be considered as an good alternative to alkanethiol-based SAMs [27,28]. An interaction similar to that between Pd clusters and the DDT surface is expected for Pd clusters on DTC or DTC2 covered surfaces, as all of these organic molecules are terminated by methyl groups. Dithiocarbamates are promising in applications for molecular electronics as well as for organic electronics and optoelectronics [29,30]. This is due to their electronic structure, bond stability and ability to functionalize metal surfaces with a wide range of substituents [30]. As dithiocarbamates have a resonant bidentate structure, they provide a molecule-metal coupling that is characteristically different compared to the one of thiols [31]. It is also noteworthy that metallization studies of DTC and DTC2 SAMs do not exist in the literature. 4-MPy SAM on the other hand was chosen for the present studies as it allows comparisons between different Pd deposition methods. A two-step electrochemical method developed by Baunach et al. [13–15] has been successfully used for Pd-metallization of 4-MPy SAMs [2,4,5,13–15,32]. The success of this method is based on the absence of the metal ions in solution and on the necessity of having the ring nitrogen facing the solution side. In this respect, we have optimal conditions to start with, when neutral Pd clusters are deposited on 4-MPy covered surfaces that have nitrogen atoms on the topmost layers. The surface structures prior to and after Pd-metallization were studied using scanning tunnelling microscopy (STM) and X-ray photoelectron spectroscopy (XPS) techniques.

2. Material and methods

2.1. SAM preparation

The SAMs of 4-MPy, DCT and DTC2 were prepared from their respective disulphide compounds whereas DDT SAM was prepared from thiol. n-Dodecanethiol (DDT, $CH_3(CH_2)_{11}SH$, purity 98%), 4,4'-dithiodipyridine ($C_{10}H_8N_2S_2$, purity 98%), tetramethylthiuram disulfide (TMTD, $(CH_3)_2NCSS_2CSN(CH_3)_2$, purity 97%) and tetraethylthiuram disulfide (TETD, $(CH_3CH_2)_2NCSS_2CSN(CH_3CH_2)_2$, purity ≥ 97%) were purchased from Sigma-Aldrich and used as received. All SAMs were prepared at room temperature (22 °C) on freshly flame-annealed Au (111) coated mica slides (300 nm Au, Georg Albert PVD). After immersions the samples were rinsed with ethanol a sufficient amount of times that XPS measurements showed a levelling in the amount of organic material on the surface. Small fluctuations in the amounts between different samples could however be observed, indicating that a small amount of excess organic molecules may still have been present on the surfaces.

- DDT SAM: Au substrate was immersed in 1 mM ethanol solution of DDT for 24 h.
- 4-MPy SAM: Au substrate was immersed in 20 μM aqueous solution of 4,4'-dithiodipyridine for 15 min.
- DTC SAM: Au substrate was immersed in 1 mM solution of TMTD (ethanol:N,N'-dimethylformamide 1:1 v/v) for 24 h.
- DTC2 SAM: Au substrate was immersed in 1 mM solution of TETD (ethanol:N,N'-dimethylformamide 10:1 v/v) for 24 h.

2.2. Cluster deposition

In the present work palladium clusters were produced with a condensation-cell-type cluster aggregation source (NC200, Oxford Applied Research), charged with a Pd target of 99.99% purity. The clusters were deposited in ultra-high vacuum at room temperature directly on the sample surfaces. The clusters are formed when Pd atoms agglomerate in argon gas (flow-rate 16 sccm). The Pd atoms exchange energy in collisions with the argon atoms, and the clusters eventually reach a velocity that is less than that of the streaming argon gas [33]. Hence, the cluster velocity v_C can be approximated to be close to the expanding gas velocity, $v_C = v_{Ar} = [2k_B T\gamma/(\gamma - 1)m_{Ar}]^{1/2}$, where γ is the heat capacity ratio for argon and equal to 5/3, k_B is the Boltzmann constant, T the gas temperature and m_{Ar} the atomic weight for argon [34]. Thus the kinetic energy E_C for the Pd clusters can be approximated to be < 0.16 eV per atom, according to $E_C = 0.5NM_C v_C^2$. All the different surfaces were uniformly deposited with Pd clusters for 15, 30, 45 and 60 s. All cluster depositions have been done using the same settings throughout all the experiments and therefore should result in the deposition of similar amounts and sizes of clusters. As a reference, transmission electron microscopy (TEM) was carried out in order to characterize the size distribution of the deposited clusters. Fig. 2(a) shows a typical TEM image from a 15 s Pd cluster deposition on a standard TEM-grid, while Fig. 2(b) shows the radial size distribution of clusters for both 15 and 60 s Pd depositions. From both the irregular shape of the upper cluster in the high-resolution inset (side length 10 nm) and the shift in the cluster size distributions going from 15 s to 60 s deposition, it can be seen that diffusion and coalescence of clusters has played an integral role in the final cluster size distributions.

2.3. Characterization

The structures were characterized by STM, HR-TEM and XPS techniques. The STM measurements were conducted in constant-current mode under ambient conditions with a Veeco Instrument NanoScope V - MultiMode V scanning probe microscope, using a Platinum/Iridium (Pt80/Ir20) wire (⌀ = 0.25 mm) as tip. The cluster size and height distribution was determined using the grain analysis function implemented in the scanning probe microscopy data analysis software Gwyddion [35].

High-resolution transmission electron microscopy (JEOL JEM-2200FS) was conducted on palladium clusters deposited on carbon

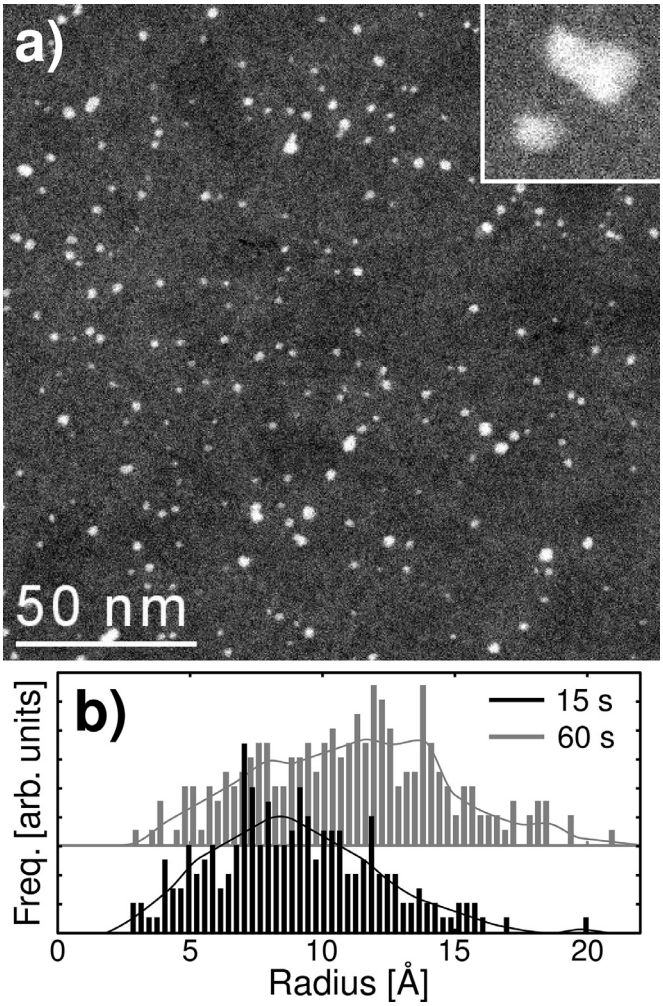

Fig. 2. a) TEM image of Pd clusters deposited on a carbon coated TEM-grid. The inset in the top right corner (side length 10 nm) shows a magnification of an irregular cluster shape. The size distributions of cluster radii, as calculated from the cluster areas, is given in b) for 15 and 60 s of Pd cluster deposition, respectively.

holey films ~ 12 nm thick (Quantifoil Micro Tools GmbH). The cluster size and distribution was determined using Gatan Microscopy Suite software for TEM analysis.

The composition and chemical state of the sample surfaces were analysed by XPS using an Argus Spectrometer (Omicron NanoTechnology GmbH, Taunusstein, Germany) operating at a pass energy of 20 eV. Samples were illuminated with X-rays emitted from a standard Mg source (K alpha line) at a photon energy of 1253.6 eV. During measurements the entire sample surface was illuminated with X-rays, while a circular aperture limited the analysis region to 0.28 mm, with electron acceptance angles of ± 1.2°. Electron emission was measured at an angle of 30°, in order to increase surface sensitivity of the measurements. This angle was varied for angle-resolved XPS measurements. Binding energies were calibrated using the Au $4f_{7/2}$ peak (84.0 eV), and peak fitting, using standard Shirley backgrounds, was done using the CasaXPS software (www.casaxps.com).

3. Results and discussion

STM studies were conducted for bare Au(111) surfaces and Au surfaces covered with DDT, DTC and DTC2 SAMs as well as for all surfaces after Pd cluster deposition. STM images typical of the sample surfaces before and after Pd cluster deposition are shown in Fig. 3. In

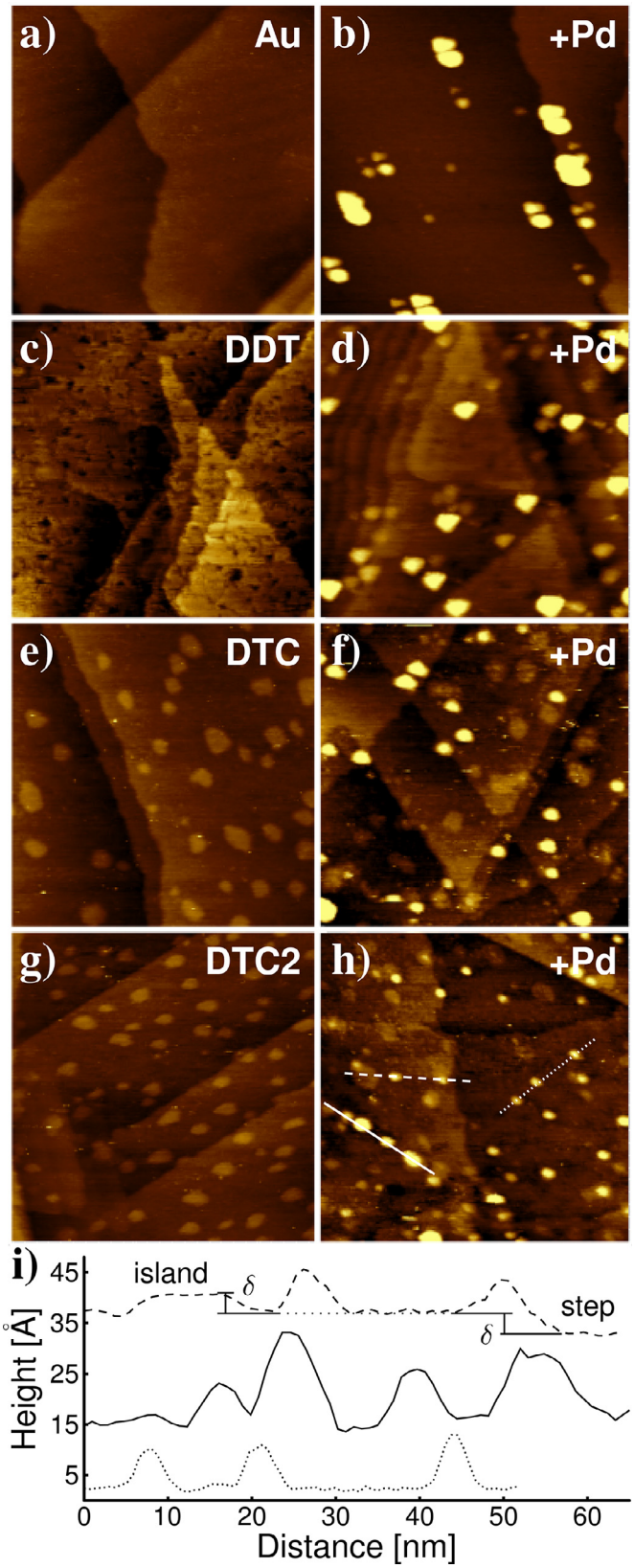

Fig. 3. a)–h) STM images before and after Pd deposition on bare Au(111), DDT, DTC, and DTC2. Side lengths are 150 nm, height scale is 1.4 nm. Line profiles from h) are shown in i). δ = 0.24 nm.

case of 4-MPy, good quality images of Pd deposited surfaces could not be obtained. Therefore the 4-MPy covered surfaces were studied solely by XPS.

Large terraces, typical of an Au(111) surface, can be seen in all images. The DDT SAM covered surface (Fig. 3(c)) is a characteristic thiolate SAM covered Au surface with 0.24 nm deep depressions that can be attributed to gold vacancy islands [36]. Substrates covered by DTC and DTC2 (Fig. 3(e) and (g)) on the other hand often exhibit nanometer-sized islands. The islands result from the interactions of dithiocarbamates and the gold surface during the SAM formation process. It has been shown that they consist of Au atoms that have been released from nearby terraces [37]. The gold islands on DTC and DTC2 surfaces have an average diameter of 10 nm and the same height ($\delta = 0.24$ nm) as atomic steps on the Au(111) substrate. Typical line profiles, showing cluster heights, as well as both step heights for the gold terraces and the gold islands can be seen in Fig. 3(i).

Pd clusters can clearly be distinguished in all post-deposition STM images (Fig. 3). Although cluster depositions have been done using the same settings throughout all the experiments and therefore should result in the deposition of similar amounts and sizes of clusters, there are clear differences between the different samples. These differences can be understood with the help of our results from the XPS measurements and are discussed later in this section.

In STM images of surfaces with clusters, lateral surface features tend to be exaggerated [38], and we have therefore given more attention to the height information available from the STM measurements. Comparison with the results from TEM analysis is not necessarily straightforward, as TEM measures projected surface area, while STM only accurately measures height. Clusters tend to diverge from a perfect spherical shape and become slightly flattened when supported by a surface. As clusters coalesce on the surface, the resulting height of the final structure will not necessarily change proportionally to the total volume of the cluster aggregate. These differences lead to slightly larger clusters as measured from lengths in TEM in comparison to clusters measured from heights in STM. Fig. 4 shows histograms of the cluster height distributions extracted from the STM images obtained for the different sample types. In Fig. 4(a) the height distributions of Au islands on the DTC and DTC2 covered surfaces and the same surfaces after Pd cluster deposition are compared. Fig. 4(b) compares the Pd cluster height distributions of the four sample types for which good-quality STM images were acquired. Measuring artefacts, such as the double tip features that can be observed in Fig. 3(b), have been accounted for during analysis of the images and their height distributions. An average of more than 300 clusters were included in the analysis for each distribution.

The total amount of Au monolayer islands that can be detected with STM on the DTC and DTC2 covered surfaces decreases once Pd clusters have been deposited (Fig. 4(a)). This decrease is more significant for the DTC SAM, possibly indicating that the Au islands might be able to act as pinning points for the clusters. When comparing the two height distributions of the Pd cluster covered surfaces, DTC exhibits a broader distribution, with increased amounts of larger clusters compared to DTC2, hinting toward a more vigorous diffusion and aggregation of clusters on the DTC surface. If clusters can freely move and aggregate until they are immobilized at step edges in the SAM structure, their resulting height distribution will contain larger clusters at the same time as the Au islands of monolayer height will be camouflaged by the larger clusters in their vicinity. Previous studies indicate that DTC2 forms more well-ordered monolayers than DTC [27,37,39]. This might be one of the reasons for the formation of a larger amount of smaller gold islands on the DTC2 surface, as can be seen in Fig. 3(g). A more well-ordered monolayer allows for less movement of the organic molecules in relation to each other once they are bound to the surface, and will therefore also limit the aggregation of gold that has been removed from step edges into large islands. A larger amount of small islands will then limit the movement of Pd clusters on the DTC2 surface, if these

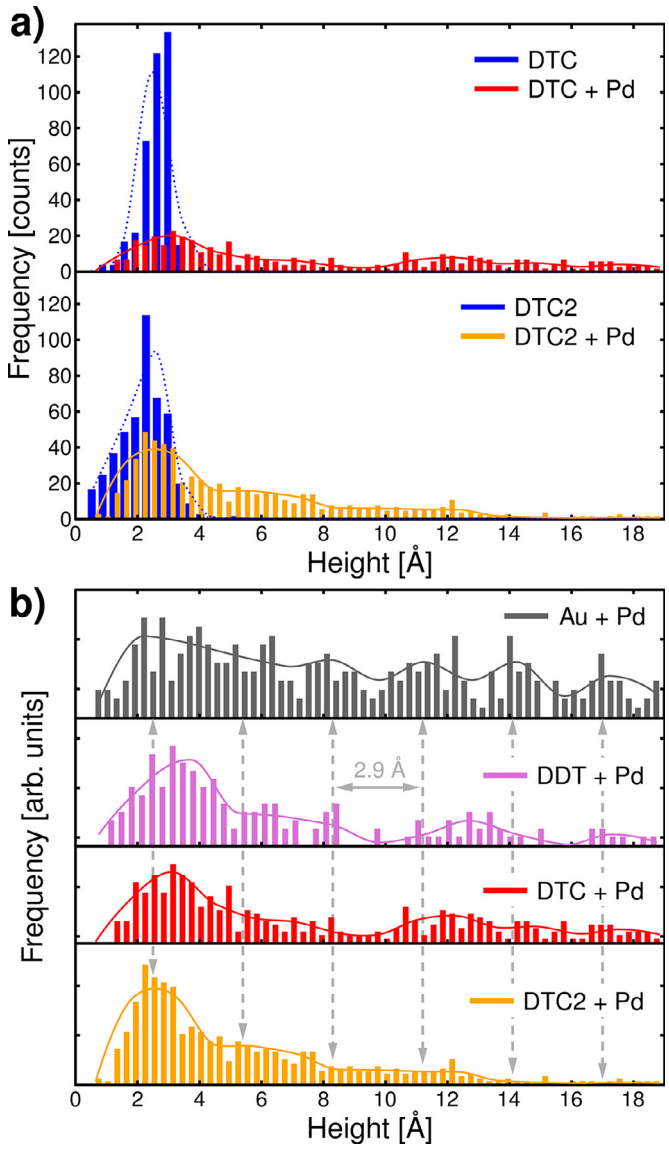

Fig. 4. a) A comparison of measured heights from the DTC and DTC2 STM images before and after a 30 s Pd deposition. b) Distribution of cluster heights acquired by STM.

islands act as pinning points.

Similar broad distributions of cluster sizes can also be seen in Fig. 4(b) for Pd clusters deposited on a bare Au substrate and on a DDT covered surface, with a substantially higher ratio of larger clusters present on the bare Au substrate. An interesting feature that can be observed for the Pd cluster distribution on bare Au substrate is a certain periodicity in the measured cluster heights. Gold and palladium are both FCC metals that have a certain affinity for each other and easily form alloys. When Pd clusters are deposited on Au(111) surfaces, they will therefore align themselves in the [111] direction, creating Pd islands with terraces made up of (111) surfaces. Although step heights on the Pd(111) surface should be approximately 2.3 Å, oxidation will cause an increase in this step height corresponding to an 18–30% expansion [40]. A periodicity of 2.9 Å can be observed in the Pd cluster height distribution for clusters deposited on a bare Au substrate, a step height corresponding to a 26% increase in the Pd(111) step height. This is in line with our XPS results which indicate that the Pd clusters have indeed oxidised after they are removed from the deposition chamber.

Dotted lines have been added to Fig. 4(b), with a periodicity of ~ 2.9 Å, highlighting the Pd cluster heights with increased frequency

on the bare Au substrate. These positions correspond to an incremental increase in the amount of (111) layers in the Pd clusters. In comparison, a similar periodicity cannot be seen for Pd clusters deposited on SAM covered surfaces. Random orientations of faceted clusters that have not aligned themselves according to the surface will result in a cluster height distribution without clearly observed step heights. Slightly larger frequencies of cluster heights at around 6, 12, and 18 Å, for Pd clusters deposited on DDT and DTC covered surfaces, may be the result of cluster aggregation, as coalescence of similar-sized clusters should result in size increases of similar increment.

Compelling evidence for the penetration of Cu and Ag clusters to a gold surface covered by DDT SAMs has previously been reported [12]. A common feature for both of these materials is that the penetrated clusters always flatten to monolayer thicknesses, forming a single-atom thick interfacial layer between the thiolate SAM and the Au surface. Such extreme flattening at the interface is not surprising, considering that even the thiol-gold interaction is strong enough to create vacancies or to remove gold atoms from step edges. A similar effect is to be expected for clusters, if strong bonds are formed between the cluster atoms and the thiols. Merely the fact that Pd clusters remain intact on the SAM covered surface would already suggest that they have not intercalcated between the gold surface and the SAM layer. In this study we have also used XPS to further analyse different samples in this respect.

XPS survey scans and high-resolution spectra of the most important peaks were collected and analysed for each sample both before and after Pd cluster deposition. Fig. 5 shows typical high-resolution spectra of the Pd 3d peaks for increasing Pd cluster deposition times. Despite an overlapping in binding energy with the Au $4d_{5/2}$ peak, the Pd peak intensities can be accurately estimated using peak fitting and fixed theoretical values for the peak area ratios and peak separation of both doublets. A linear increase in Pd amounts could be measured for all samples as a function of Pd cluster deposition times. Pd $3d_{5/2}$ energies at 335.4 eV agree with previously measured energies for Pd oxides on Pd particles [41]

Fig. 6 shows typical C 1s, S 2p, and N 1s peaks, where relevant for each of the different types of SAM-covered samples, both before (darker colours) and after (lighter colours) Pd cluster deposition. As can be seen from the C 1s spectra collected from the bare Au substrate, a significant amount of adventitious carbon is present on the sample, with a typical dominance of C–C or C–H bonded carbon at a binding energy of

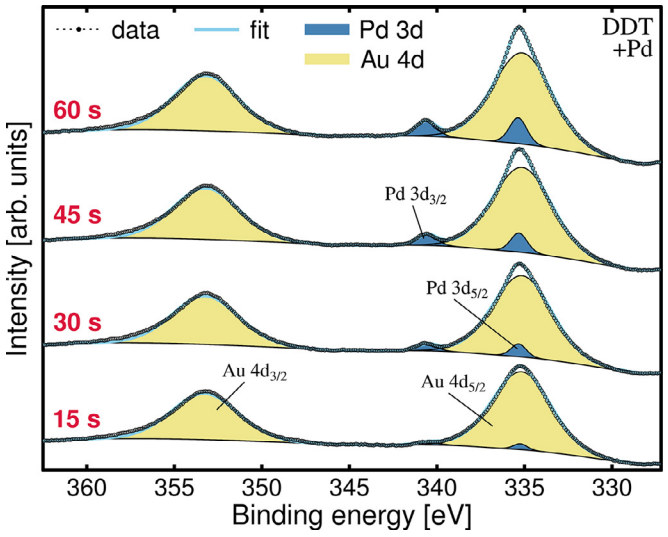

Fig. 5. High-resolution XPS peaks for the Pd 3d and overlapping Au 4d. With the help of peak fitting, individual peaks for both doublets have been estimated, showing a linear increase in the amount of Pd as cluster deposition times are increased.

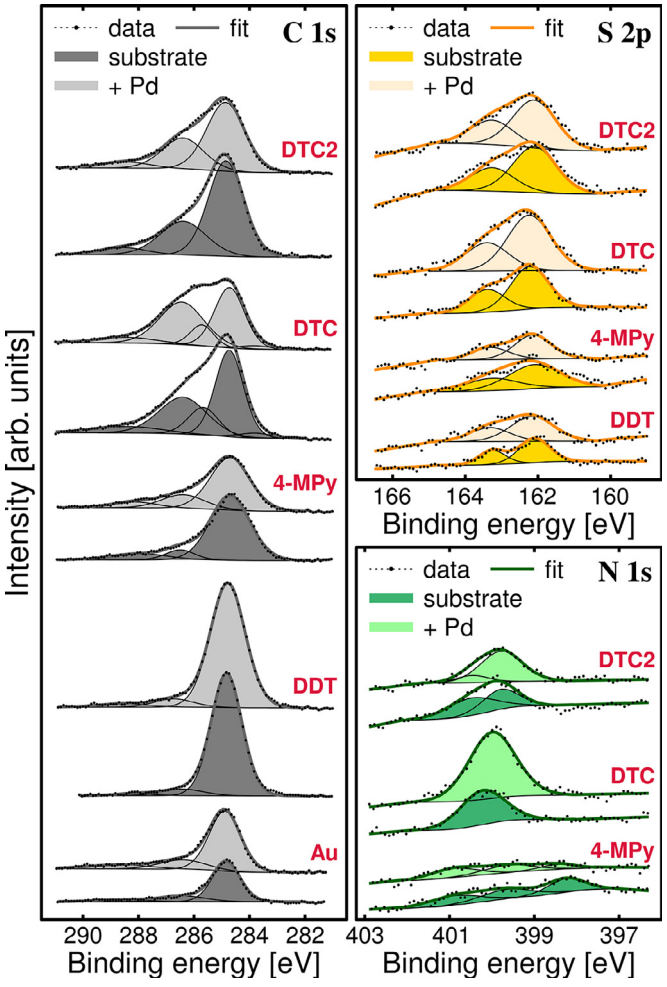

Fig. 6. High-resolution XPS peaks of C 1s, S 2p, and N 1s core-levels, for bare Au and organic SAM-covered surfaces, both before (darker colours) and after (lighter colours) 60 s Pd cluster deposition. No major shifts in binding energy can be seen for samples before and after deposition. Carbon spectra are dominated by the typical C–C or C–H bonding that appears at 284.8 eV, while sulphur spectra show typical bound thiolate sulphur signals with the S $2p_{3/2}$ peak located at 162.1 eV. For DTC and DTC2 nitrogen spectra show thioamide- and amine-like bonding at 399.8 eV and 401.0 eV, respectively. 4-MPy exhibits both typical pyridinic nitrogen at 398.5 eV, as well as higher binding energies at 399.8 eV and 400.7 eV. (For interpretation of the references to colour in this figure legend, the reader is referred to the web version of this article.)

284.8 eV. Although a similar presence of carbon contamination is to be expected for the other substrate types as well, as all samples have been exposed to the ambient, the strong carbon signal from the SAMs is evident through the appearance of higher energy peaks related to a more complex carbon bonding in the 4-MPy, DTC, and DTC2 thiolates.

The S 2p spectra for all SAM-containing samples showed typical bound thiolate sulphur signals, with the S $2p_{3/2}$ peak located at 162.1 eV. No unbound thiols, with typical binding energies of about 164 eV [11], could be detected. Among the nitrogen containing thiolates, 4-MPy, as expected, contains a large amount of pyridinic nitrogen with a binding energy of approximately 398.5 eV, but also almost equally strong signals at higher energies, in accordance with previous XPS measurements [42]. For the case of DTC and DTC2 samples, thioamide- and amine-like bonding appear at 399.8 eV and 401.0 eV respectively.

The most important finding from Fig. 6, however, is that despite the differences between the various types of samples, no major changes can be detected between substrates before and after Pd cluster deposition. A lack of changes in carbon binding energies was to be expected, as the

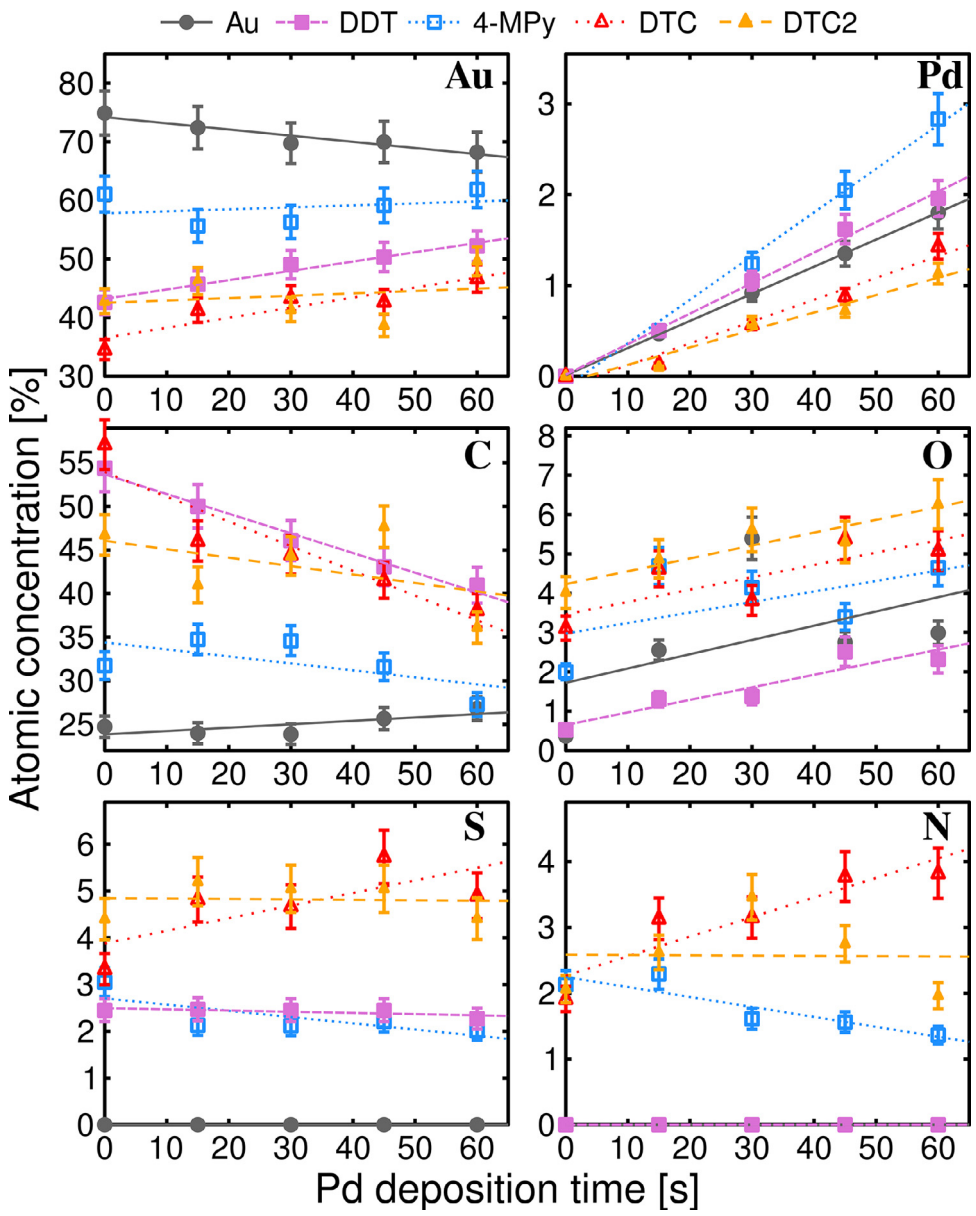

Fig. 7. XPS analysis results shown as the atomic concentrations of elements detected in the samples. A bare Au surface and Au surfaces coated with SAMs were analysed before Pd deposition and after depositions of 15, 30, 45 and 60 s. Linear fits have been adapted as a first approximation. Error bars represent the combined standard deviation from both peak fitting and measurements on at least three different samples for every substrate type.

thiols should remain unaltered as a result of the deposition of metal clusters. For the case of sulphur and nitrogen, however, changes in binding energies could occur, either if cluster atoms penetrate through the thiol layer and alter the S—Au bond, or if a strong bonding occurs with the nitrogen groups of nitrogen containing thiols. Since no shifts in the binding energies for these elements can be detected, it is safe to assume that only weak van der Waals type bonding occurs between the Pd clusters and the thiolate SAMs.

High-resolution spectra of the O 1s, Au 4f, and Pd 3d core-level peaks were also included in an analysis of the relative amounts of elements on the surface of the samples. For each type of sample the average relative amount of each element as a function of Pd cluster deposition time is plotted in Fig. 7. Linear fits have been made to all of the data, and as a first approximation these tend to represent the observed trends fairly well. The few deviations that occur are most noticeable for the carbon concentration on 4-MPy samples, and for the nitrogen content on DTC2, both of which appear to reach a maximum after about 30 s of Pd cluster deposition. Although more complex quantitative models could be adopted in order to explain these discrepancies, linear fits are suitable for a qualitative discussion of the results.

For the bare Au surface (grey solid line with solid dots), the relative amount of Au decreases with increasing amounts of Pd. Coupled with the Pd increase is an increase in the relative amount of oxygen and a slight increase in the amount of carbon. The most likely reason for this is an oxidation of the Pd clusters upon introduction to the ambient and a slight increase in the amount of impurity carbon that binds to the partially oxidized surface. For all the other sample types, a similar increase in oxygen can be measured with increasing Pd coverage. A large discrepancy can however be seen for the behaviour of the relative amounts of gold when the Pd content is increased on the SAM covered surfaces.

Opposite to what is the case for the bare Au substrate, the relative amount of Au that can be measured by XPS, somewhat surprisingly, increases when the amount of deposited Pd is increased. This is very counter-intuitive, as the escape depth for photoelectrons is typically

only in the order of a few nanometers, and XPS peak intensities from elements in the surface therefore normally decrease even if very little material is deposited on the samples. One possible explanation for this behaviour is that the thiolates on the SAM covered surfaces are attracted so strongly by the deposited Pd clusters that they agglomerate beneath the clusters at higher densities than they normally cover the Au surface. This can occur on the SAM layers that typically include several types of intrinsic and extrinsic defects, such as grain boundaries or vacancy islands and exposed thiol chains at step edges in the underlying gold substrate [9,26]. Similar defects will lower the global density of the organic molecules, even though a local highly packed structure exists. Through this process some gold from the substrate would be uncovered, leading to higher intensities of the Au 4f peak. This is partly supported by the behaviour of the carbon intensities, which decrease dramatically for all SAM covered samples with increasing Pd concentrations. Slight decreases in the carbon amount is to be expected if the Pd clusters remain on top of the thiolate layer, but what can be observed for all samples is an unproportionally large decrease in the total carbon concentration.

The relative amount of sulphur, as measured by XPS, decreases for both DDT (dashed line with solid squares) and 4-MPy (dotted line with hollow squares) samples, as does the amount of nitrogen for 4-MPy. For 4-MPy the relative decrease in nitrogen is higher than the corresponding decrease in sulphur, indicating that the Pd clusters indeed are bonded to the nitrogen groups that bend toward the clusters, and therefore shield the photoelectron signal from nitrogen slightly more than that from sulphur. With DTC (dotted line with hollow triangles) and DTC2 (dashed line with solid triangles) matters are more complicated. For the case of DTC2, both sulphur and nitrogen concentrations decrease only very slightly, whereas for DTC both signals actually increase with increased Pd cluster amounts. Coupled together with the decrease in carbon, this is indeed surprising, as this would indicate that somehow the carbon in the thiols is shielded by the deposited Pd more than nitrogen and sulphur, which, for the case of DTC, are even slightly uncovered upon Pd cluster deposition. As can be seen in Fig. 1, however, most of the carbon in DTC and DTC2 is located at the upper end of the thiols, whereby thiol attraction to the Pd clusters could uncover more of the underlying sulphur and nitrogen.

Another interesting feature can be seen from the relative Pd concentrations presented in the graph at the top-most, right-hand corner of Fig. 7. For all sample types the amount of Pd increases linearly with deposition time, which is to be expected as all depositions were done at constant rate. However, although the deposition parameters have been the same for all sample types, the relative amounts of palladium grow at very different rates, with the measured intensities at their largest (greater than the signal from Pd clusters on bare gold substrates) for 4-MPy and DDT, and smallest (below those of bare gold) for DTC and DTC2. If the intensities measured on the bare gold substrate are taken as a standard, larger palladium intensities can be explained by lowered diffusion and agglomeration rates for the deposited clusters. XPS signals, measured from samples containing the same volume of a certain element will be lower if this appears in larger particles. This is due to a self-shielding effect, as photoelectrons from lower parts of a particle can be scattered by the material that is covering it, thereby resulting in a relatively weaker signal from the cluster material, even though it is contained on the surface in equal amounts. Smaller particles will therefore usually result in larger XPS signals even if the total amount of the element on the sample surface is the same. From Fig. 4(b) it can be seen that the size distribution of clusters on the bare gold surfaces tends to contain larger clusters than distributions on other surfaces.

Lower intensities for similar sizes, on the other hand, can be explained by a partial covering of the Pd clusters on the surfaces. The size distribution in Fig. 4(b) for DTC2 contains on average considerably smaller clusters than the other samples, which should lead to the largest XPS signal for palladium. Quite the contrary, however, can be seen in Fig. 7, where these samples provide the lowest palladium signals. Smaller clusters, and therefore a lower likelihood for diffusion and agglomeration of the clusters can be explained by a strong cluster-thiol interaction, or even a partial covering of the clusters upon impact. A larger amount of small gold islands on the DTC2 covered surface will also result in more step edges, where thiols on upper terraces can tilt toward the deposited clusters and thereby slightly shield them, resulting in lower XPS signals. All substrates containing SAMs on gold lead to cluster size distributions with, on average, smaller clusters than that of clusters on bare gold. Differences in palladium XPS intensities between the SAM-covered substrates can then mainly be explained by different strengths of bonding and a partial covering of the clusters with thiols.

The rate of increase in Pd 3d intensities as a function of deposition time (top-most, right-hand corner of Fig. 7) can be understood as being inversely related to the strength of bonding between the Pd clusters and the thiol layer. This is also in agreement with the observed trend of the XPS measured intensities for sulphur and nitrogen, as a stronger bonding and partial covering of the clusters with thiols should lead to a slower decrease in concentration. According to this, the weakest bonding should occur between the Pd clusters and the 4-MPy SAM, a finding which is supported by the difficulties in achieving good STM images of these samples. The deposited clusters were very loosely bound to the surface, and therefore reacted heavily with the STM tip during measurements, occasionally sticking to the tip and causing critical noise and imaging artefacts that diminished the quality of the images. The interaction is then slightly stronger for DDT, and very strong for DTC and DTC2. Because of the complex nature of the system, a precise relationship for the bonding strength of the different systems cannot easily be determined and is out of the scope this study. A qualitative assessment is however validated by the evidence provided here.

Angle-resolved XPS measurements were also done in order to provide further evidence on the ordering between the Pd/SAM layers. Fig. 8(a) and (b) show N 1s and Pd $3d_{3/2}$ spectra collected at different electron emission angles from a sample with a 4-MPy SAM onto which Pd clusters have been deposited for 60 s. Each spectrum has been normalized by the total combined intensity from N 1s and Pd $3d_{3/2}$ core levels in order to facilitate an easier comparison between the spectra. In angle-resolved XPS the angle at which emitted photoelectrons are

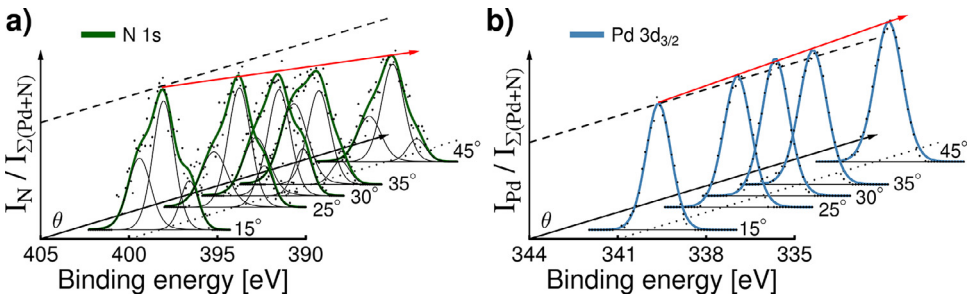

Fig. 8. a) N 1s and b) Pd $3d_{3/2}$ spectra collected at different electron emission angles from a sample with a 4-MPy SAM onto which Pd clusters have been deposited for 60 s. All spectra have been normalized by the total combined intensity from N 1s and Pd $3d_{3/2}$ core levels in order to facilitate an easier comparison between the spectra. Vertical axes therefore show the relative intensities in arbitrary units, while binding energy is given on the horizontal axes. Dashed lines indicate constant relative intensities, while dotted lines indicate constant binding energies. The third axis of each graph shows photoelectron emission angles θ. Red arrows highlight how the photoemission intensity varies with θ, indicating that relative Pd signals increase and relative N signals decrease at greater emission angles.

collected is changed, resulting in differences in total depth of the sample that is probed. When measurements are done at a higher angle of deviation from the surface normal, the total depth from which photoelectrons can escape the surface and reach the analyser is decreased, thereby allowing for a greater portion of the measured XPS signal to come from the surface layers of the sample. When comparing the intensities of two different elements in the sample, the element that is situated closer to the surface will usually exhibit a larger relative signal at greater emission angles. Elemental concentrations are estimated from the entire area of a photoemission peak, but for peak shapes that are similar enough, a comparison between peak heights will also give an indication of the changes in magnitude of the total photoemission intensity.

The dashed lines in Fig. 8(a) and (b) indicate constant relative intensity levels for N 1s and Pd $3d_{3/2}$ photoemission signals, whereas the red arrows highlight how these relative signals deviate from a constant value as the electron emission angle is increased. The relative intensity of N decreases for greater angles, while the relative intensity of Pd increases. This indicates that, in a comparison between Pd and N, the majority of Pd is situated in the upper surface layers of the sample, while N is located in the layers below these.

Similar measurements were done for samples from all four types of surfaces onto which Pd clusters had been deposited for 60 s. Fig. 9 shows the relative changes in the ratios between concentrations of Pd and S ($\Delta C_{Pd}/C_S$) in Fig. 9(a), Pd and N ($\Delta C_{Pd}/C_N$) in Fig. 9(b), and N and S ($\Delta C_N/C_S$) in Fig. 9(c). All ratios are compared to those measured at an angle of 30°. Linear fits are included as a guide to the eye. Error bars are standard deviations calculated from the fitting procedures in CasaXPS.

From Fig. 9(a) and (b) it can be seen that the relative strength of the Pd signal increases as compared to both S and N signals when the emission angle is increased. This is strong evidence toward the Pd clusters being located on top of the organic SAM layers, as these are the only sources of S and N in the samples. An interesting feature is that the relative increases are similar for the Pd/N ratios in all N-containing SAMs, while considerably higher rates of increase in the Pd/S ratios can be observed for DTC and DTC2, which both contain two sulphur atoms for every molecule as compared to only one for each organic molecule in DDT and 4-MPy. When comparing the N/S ratio in 4-MPy, DTC, and DTC2, the expected increase in the ratio with increased emission angles can be observed for DTC and DTC2, indicating that sulphur atoms are indeed bonded to the gold surface and nitrogen atoms are facing the ambient or Pd side of the sample. For the case of 4-MPy, however, a fairly constant ratio between N and S can be observed, even though the collection angle for emitted photoelectrons is increased. Taken together with the fact that STM imaging of the 4-MPy surfaces was found difficult, this seems to point toward a great disorder in the 4-MPy layer. Despite this, when comparing the Pd signal intensity to N and S, it would appear that the 4-MPy SAMs have nonetheless been impenetrable to the Pd clusters.

4. Conclusions

As most of the clusters on the SAM covered gold surfaces are higher than monolayer islands, it is fair to assume that they have not penetrated through the organic layers, where the strong interaction between the thiols and the gold usually leads to a rapid flattening of multilayer islands. Contrary to what can be measured for Pd clusters on bare Au substrates, a clear periodicity in the height distributions of the clusters deposited on these self-assembled organic layers cannot be seen. The SAM supported clusters have smaller sizes due to a decreased aggregation, presumably caused by lower rates of diffusion on the thiolate layer. Clusters supported by the organic layers have random orientations, and their height distributions will therefore not contain discrete increments in size, in a manner similar to the epitaxially aligned

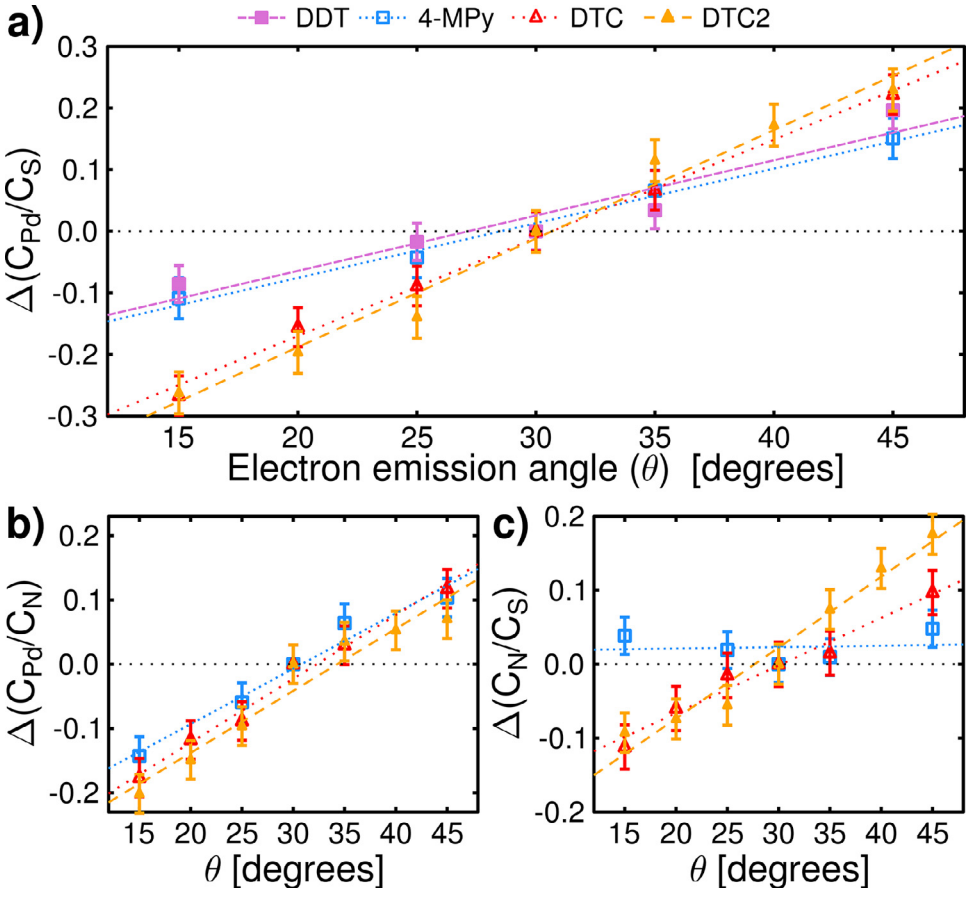

Fig. 9. Changes in the relative ratios between XPS intensities for a) Pd and S, b) Pd and N, and c) N and S when measured and different photoelectron emission angles. Relative increases in Pd as compared to S and N indicate that Pd clusters are situated above the organic SAM layers. Increased relative amounts of N as compared to S indicate that the SAM layers have formed with sulphur bound to the gold substrate and nitrogen facing the ambient. The vertical axes indicate relative changes in the ratios between elements, as compared to those measured at an angle of 30°. Linear fits are included as a guide to the eye. Error bars are standard deviations calculated from the fitting procedures.

clusters that have been deposited on bare Au substrates.

Uncharacteristic increases in the XPS intensities of the Au 4f peaks, coupled with decreases in the C 1s intensities, show that photoelectrons from the thiolates are screened, while some of the Au surface is uncovered due to thiol-Pd interactions. Different rates of linear increase in Pd 3d intensities, for the same amount of deposited clusters, are most likely due to differences in the strength of bonding between Pd clusters and the various thiolates. A partial covering of the clusters with organic material is most likely the reason for lower Pd intensities for some substrates. According to this the bonding strength between Pd clusters and thiols is the lowest for clusters on 4-MPy, and then increases for each of DDT, DTC and DTC2. Angle-resolved XPS measurements further point toward the Pd clusters being situated on top of the organic SAMs.

Our findings strongly point toward SAMs of DDT, 4-MPy, DTC, and DTC2 being impenetrable for Pd clusters deposited at thermal energies. Contrary to most methods of metallization, cluster deposition therefore efficiently allows for the growth of metal overlayers on organic SAMs, without the formation of metallic shorts or unwanted interfacial layers. Deposition of preformed metal clusters efficiently hinders the penetration of metal adatoms through the thiolate layers, as all deposited atoms are bound to the clusters, thereby limiting their ability to diffuse on the surface and leak through defects or other parts of the film.

Acknowledgments

The doctoral program in Materials Research and Nanosciences (MATRENA) of Helsinki University is acknowledged for financial support.

Funding

Funding from the Finnish Center of Excellence in Atomic Layer Deposition (Academy of Finland) is gratefully acknowledged.

Supplementary material

Supplementary material associated with this article can be found, in the online version, at doi:10.1016/j.susc.2018.06.006.

References

[1] X. Dong, Y. Xia, G. Zhu, B. Zhang, Molecular sensing with the tunnel junction of an Au nanogap in solution, Nanotechnology 18 (39) (2007) 395502, http://dx.doi.org/10.1088/0957-4484/18/39/395502. http://stacks.iop.org/0957-4484/18/i=39/a=395502?key=crossref.cc926a097af57459c48fe76d2438b55b .

[2] H.-G. Boyen, P. Ziemann, U. Wiedwald, V. Ivanova, D.M. Kolb, S. Sakong, A. Gross, A. Romanyuk, M. Büttner, P. Oelhafen, Local density of states effects at the metal-molecule interfaces in a molecular device, Nat. Mater. 5 (5) (2006) 394–399, http://dx.doi.org/10.1038/nmat1607.

[3] A. Gross, Adsorption at nanostructured surfaces from first principles, J. Comput. Theor. Nanosci. 5 (5) (2008) 894–922.

[4] O. Shekhah, C. Busse, A. Bashir, F. Turcu, X. Yin, P. Cyganik, A. Birkner, W. Schuhmann, C. Wöll, Electrochemically deposited Pd islands on an organic surface: the presence of Coulomb blockade in STM I(V) curves at room temperature, Phys. Chem. Chem. Phys. 8 (29) (2006) 3375–3378, http://dx.doi.org/10.1039/b606488d. http://www.ncbi.nlm.nih.gov/pubmed/16855713 .

[5] J. Kučera, A. Groß, Reduced Pd density of states in Pd/SAM/Au junctions: the role of adsorbed hydrogen atoms, Phys. Chem. Chem. Phys. 14 (7) (2012) 2353, http://dx.doi.org/10.1039/c2cp22740a.

[6] S. Duffe, N. Grönhagen, L. Patryarcha, B. Sieben, C. Yin, B. von Issendorff, M. Moseler, H. Hövel, Penetration of thin C60 films by metal nanoparticles, Nat. Nanotechnol. 5 (5) (2010) 335–339, http://dx.doi.org/10.1038/nnano.2010.45.

[7] M.T. Nakaya, Molecular electronics: formation and control of ultrasharp metal/molecule interfaces by controlled immobilization of sizeselected metal nanoclusters onto organic molecular films, Adv. Funct. Mater. 24 (2014), http://dx.doi.org/10.1002/adfm.201470053.

[8] M. Nakaya, T. Iwasa, H. Tsunoyama, T. Eguchi, A. Nakajima, Formation of a superatom monolayer using gas-phase-synthesized Ta@Si16 nanocluster ions, Nanoscale 6 (24) (2014) 14702–14707, http://dx.doi.org/10.1039/C4NR04211E.

[9] J.C. Love, L.A. Estroff, J.K. Kriebel, R.G. Nuzzo, G.M. Whitesides, Self-assembled monolayers of thiolates on metals as a form of nanotechnology, Chem. Rev. 105 (4) (2005) 1103–1169, http://dx.doi.org/10.1021/cr0300789. http://www.ncbi.nlm.nih.gov/pubmed/15826011 .

[10] C. Silien, M. Buck, On the role of extrinsic and intrinsic defects in the underpotential deposition of Cu on thiol-modified Au(111) electrodes, J. Phys. Chem. C 112 (10) (2008) 3881–3890, http://dx.doi.org/10.1021/jp710947r.

[11] A.V. Walker, T.B. Tighe, O.M. Cabarcos, M.D. Reinard, B.C. Haynie, S. Uppili, N. Winograd, D.L. Allara, The dynamics of noble metal atom penetration through methoxy-terminated alkanethiolate monolayers, J. Am. Chem. Soc. 126 (12) (2004) 3954–3963, http://dx.doi.org/10.1021/ja0395792.

[12] L. Costelle, M.T. Raisanen, J.T. Joyce, C. Silien, L.-S. Johansson, J.M. Campbell, J. Raisanen, Structural evolution of gas-phase coinage metal clusters in thiolate self-assembled monolayers on Au, J. Phys. Chem. C 116 (42) (2012) 22602–22607, http://dx.doi.org/10.1021/jp307148p.

[13] T. Baunach, V. Ivanova, D.M. Kolb, H.-G. Boyen, P. Ziemann, M. Büttner, P. Oelhafen, M. Büttner, P. Oelhafen, A new approach to the electrochemical metallization of organic monolayers: palladium deposition onto a 4,4'-dithiodipyridine self-assembled monolayer, Adv. Mater. 16 (22) (2004) 2024–2028, http://dx.doi.org/10.1002/adma.200400409.

[14] V. Ivanova, T. Baunach, D.M. Kolb, Metal deposition onto a thiol-covered gold surface: a new approach, Electrochim. Acta 50 (21) (2005) 4283–4288, http://dx.doi.org/10.1016/j.electacta.2005.05.047. http://linkinghub.elsevier.com/retrieve/pii/S0013468605006067 .

[15] M. Manolova, V. Ivanova, D. Kolb, H.-G. Boyen, P. Ziemann, M. Büttner, A. Romanyuk, P. Oelhafen, Metal deposition onto thiol-covered gold: platinum on a 4-mercaptopyridine SAM, Surf. Sci. 590 (2–3) (2005) 146–153, http://dx.doi.org/10.1016/j.susc.2005.06.005. http://linkinghub.elsevier.com/retrieve/pii/S0039602805006278 .

[16] H. Kind, A.M. Bittner, O. Cavalleri, K. Kern, T. Greber, Electroless deposition of metal nanoislands on aminothiolate-functionalized Au(111) electrodes, J. Phys. Chem. B 102 (39) (1998) 7582–7589, http://dx.doi.org/10.1021/jp981684o.

[17] E.A. Speets, P. te Riele, M.A.F. van den Boogaart, L.M. Doeswijk, B.J. Ravoo, G. Rijnders, J. Brugger, D.N. Reinhoudt, D.H.A. Blank, Formation of metal nano- and micropatterns on self-assembled monolayers by pulsed laser deposition through nanostencils and electroless deposition, Adv. Funct. Mater. 16 (10) (2006) 1337–1342, http://dx.doi.org/10.1002/adfm.200500933.

[18] F. Camacho-Alanis, L. Wu, G. Zangari, N. Swami, Molecular junctions of 1 nm device length on self-assembled monolayer modified n- vs. p-GaAs, J. Mater. Chem. 18 (45) (2008) 5459, http://dx.doi.org/10.1039/b811395e.

[19] M.I. Muglali, A. Bashir, A. Birkner, M. Rohwerder, Hydrogen as an optimum reducing agent for metallization of self-assembled monolayers, J. Mater. Chem. 22 (29) (2012) 14337, http://dx.doi.org/10.1039/c2jm32111d.

[20] E.A. Speets, B. Dordi, B.J. Ravoo, N. Oncel, A.-S. Hallbäck, H.J.W. Zandvliet, B. Poelsema, G. Rijnders, D.H.A. Blank, D.N. Reinhoudt, Noble metal nanoparticles deposited on self-assembled monolayers by pulsed laser deposition show coulomb blockade at room temperature, Small 1 (4) (2005) 395–398, http://dx.doi.org/10.1002/smll.200400126. http://www.ncbi.nlm.nih.gov/pubmed/17193461 .

[21] E.A. Speets, B.J. Ravoo, F.J.G. Roesthuis, F. Vroegindeweij, D.H.A. Blank, D.N. Reinhoudt, Fabrication of arrays of gold islands on self-assembled monolayers using pulsed laser deposition through nanosieves, Nano Lett. 4 (5) (2004) 841–844, http://dx.doi.org/10.1021/nl049774u.

[22] C. Winter, U. Weckenmann, R.A. Fischer, .J. Käshammer, V. Scheumann, S. Mittler, Selective nucleation and area-selective OMCVD of gold on patterned self-assembled organic monolayers studied by AFM and XPS: a comparison of OMCVD and PVD, Chem. Vap. Deposition 6 (4) (2000) 199–205, http://dx.doi.org/10.1002/1521-3862(200008)6:4<199::AID-CVDE199>3.0.CO;2-2.

[23] L. Costelle, T.T. Jarvi, M.T. Raisanen, V. Tuboltsev, J. Raisanen, Binding of deposited gold clusters to thiol self-assembled monolayers on Au(111) surfaces, Appl. Phys. Lett. 98 (4) (2011) 043107, http://dx.doi.org/10.1063/1.3548862.

[24] J. van Lith, A. Lassesson, S.A. Brown, M. Schulze, J.G. Partridge, A. Ayesh, A hydrogen sensor based on tunneling between palladium clusters, Appl. Phys. Lett. 91 (18) (2007) 181910, http://dx.doi.org/10.1063/1.2802730.

[25] R. Wsuurschum, K. Reimann, S. Grub, A. Ksuubler, P. Scharwaechter, W. Frank, O. Kruse, H.D. Carstanjen, H.-E. Schaefer, Structure and diffusional properties of nanocrystalline Pd, Philos. Mag. Part B 76 (4) (1997) 407–417, http://dx.doi.org/10.1080/01418639708241104.

[26] C. Vericat, M.E. Vela, R.C. Salvarezza, Self-assembled monolayers of alkanethiols on Au(111): surface structures, defects and dynamics, Phys. Chem. Chem. Phys. 7 (18) (2005) 3258–3268, http://dx.doi.org/10.1039/b505903h.

[27] H. Zhu, D.M. Coleman, C.J. Dehen, I.M. Geisler, D. Zemlyanov, J. Chmielewski, G.J. Simpson, A. Wei, Assembly of dithiocarbamate-anchored monolayers on gold surfaces in aqueous solutions, Langmuir 24 (16) (2008) 8660–8666, http://dx.doi.org/10.1021/la801254b.

[28] Y. Zhao, W. Pérez-Segarra, Q. Shi, A. Wei, Dithiocarbamate assembly on gold, J. Am. Chem. Soc. 127 (20) (2005) 7328–7329, http://dx.doi.org/10.1021/ja050432f.

[29] J.M. Wessels, H.-G. Nothofer, W.E. Ford, F. von Wrochem, F. Scholz, T. Vossmeyer, A. Schroedter, H. Weller, A. Yasuda, Optical and electrical properties of three-Dimensional interlinked gold nanoparticle assemblies, J. Am. Chem. Soc. 126 (10) (2004) 3349–3356, http://dx.doi.org/10.1021/ja0377605.

[30] F. von Wrochem, D. Gao, F. Scholz, H.-G. Nothofer, G. Nelles, J.M. Wessels, Efficient electronic coupling and improved stability with dithiocarbamate-based molecular junctions, Nat. Nanotechnol. 5 (8) (2010) 618–624, http://dx.doi.org/10.1038/nnano.2010.119.

[31] P. Morf, F. Raimondi, H.-G. Nothofer, B. Schnyder, A. Yasuda, J.M. Wessels, T.A. Jung, Dithiocarbamates: functional and versatile linkers for the formation of self-assembled monolayers, Langmuir 22 (2) (2006) 658–663, http://dx.doi.org/10.1021/la052952u.

[32] M. Saitner, F. Eberle, J. Baccus, M. D'Olieslaeger, P. Wagner, D.M. Kolb, H.-G. Boyen, Impact of functional groups onto the electronic structure of metal electrodes in molecular junctions, J. Phys. Chem. C 116 (41) (2012) 21810–21815, http://dx.doi.org/10.1021/jp3059596.

[33] H. Haberland (Ed.), Clusters of atoms and molecules, Springer Series in Chemical Physics, vol. 52, Springer Berlin Heidelberg, Berlin, Heidelberg, 1994, , http://dx.doi.org/10.1007/978-3-642-84329-7.
[34] I. Yamada, N. Toyoda, Recent advances in R&D of gas cluster ion beam processes and equipment, Nucl. Instrum. Methods Phys. Res. Sect. B 241 (1–4) (2005) 589–593, http://dx.doi.org/10.1016/j.nimb.2005.07.076. http://linkinghub.elsevier.com/retrieve/pii/S0168583X05012814 .
[35] P. Klapetek, D. Necas Gwyddion, 2014. http://gwyddion.net/.
[36] J.-P. Bucher, L. Santesson, K. Kern, Thermal healing of self-assembled organic monolayers: hexane- and octadecanethiol on Au(111) and Ag(111), Langmuir 10 (4) (1994) 979–983, http://dx.doi.org/10.1021/la00016a001.
[37] A.F. Raigoza, G. Kolettis, T.E.S. Brandt, G. Caponigri-Guerra, C. Agostino, S.A. Kandel, Coadsorption of octanethiol and dialkyldithiocarbamate on Au(111), J. Phys. Chem. C 116 (2) (2012) 1930–1934, http://dx.doi.org/10.1021/jp2110538.
[38] K. Birdi, Scanning Probe Microscopes, CRC Press, 2003, http://dx.doi.org/10.1201/9780203011072.
[39] P. Morf, N. Ballav, M. Putero, F. von Wrochem, J.M. Wessels, T.A. Jung, Supramolecular structures and chirality in dithiocarbamate self-assembled monolayers on Au(111), J. Phys. Chem. Lett. 1 (5) (2010) 813–816, http://dx.doi.org/10.1021/jz900435w.
[40] D. Zhang, C. Jin, H. Tian, Y. Xiong, H. Zhang, P. Qiao, J. Fan, Z. Zhang, Z.Y. Li, J. Li, An In situ TEM study of the surface oxidation of palladium nanocrystals assisted by electron irradiation, Nanoscale 9 (19) (2017) 6327–6333, http://dx.doi.org/10.1039/C6NR08763A.
[41] K. Noack, H. Zbinden, R. Schlögl, Identification of the state of palladium in various hydrogenation catalysts by XPS, Catal. Lett. 4 (2) (1990) 145–155, http://dx.doi.org/10.1007/BF00765697.
[42] J. Poppenberg, S. Richter, E. Darlatt, C.H.-H. Traulsen, H. Min, W.E. Unger, C.A. Schalley, Successive coordination of palladium(II)-ions and terpyridine-ligands to a pyridyl-terminated self-assembled monolayer on gold, Surf. Sci. 606 (3–4) (2012) 367–377, http://dx.doi.org/10.1016/j.susc.2011.10.020. http://linkinghub.elsevier.com/retrieve/pii/S0039602811004250 .